JOURNAL OF THERMOPHYSICS AND HEAT TRANSFER
Vol. 9, No. 2, April–June 1995

Solutal Convection and Mass Transfer in Inclined Enclosures

C. Gau* and D. Z. Jeng†
National Cheng Kung University, Tainan, Taiwan 70107, Republic of China

Both experimental and numerical work are performed to study the solutal convection flow and transport process in the enclosures that can be inclined at different angles. The enclosure is filled with an aqueous solution containing $CuSO_4 + H_2SO_4$, where the flow structure is visualized by both a particle tracer and shadowgraph. With a nonintrusive optical method the concentration fluctuations at desired locations are measured. The mass transfer Sherwood numbers across the enclosure at various inclinations are also measured and the results are correlated in terms of relevant nondimensional parameters. In the experiments, the Rayleigh number ranges from 1.126×10^8 to 1.157×10^{11}, the Schmidt numbers from 2500 to 3989, the angles of inclination from 30 to 150 deg, and the aspect ratios of the enclosure from 0.25 to 1. The SIMPLE algorithm developed by Patankar is employed to calculate the solutal convection, and the results are compared with the data. It was found that both the inclination and the aspect ratio of the enclosure have a significant effect on the flow structure and mass transfer. For a large angle of inclination, the accumulation of solutal boundary-layer flow leads to stratification of the core and reduction of the mass transfer. For a small inclination, generation and protrusion of solutal plumes leads to oscillation of concentration and enhancement of mass transfer.

Nomenclature

A = area
AR = aspect ratio, H/L
C = concentration of cupric ion
D = solutal diffusivity
F = Faraday constant
Gr = Grashof number, $g\beta_s(C_a - C_c)H^3/\nu^2$
g = gravitational acceleration or gram
H = height of the enclosure
h_s = convective mass transfer coefficient
i = average current density
k = thermal conductivity
L = width of the enclosure
M = molarity
m = mass
p = pressure
q'' = mass flux, it_2/z_1 F
Ra = solutal Rayleigh number, $g\beta_s(C_a - C_c)H^3/\nu D$
Sc = Schmidt number
Sh = Sherwood number, h_sH/D
T = temperature
t = time
t_2 = transference number
u = velocity in x direction
v = velocity in y direction
x = coordinate normal to the electrodes
y = coordinate parallel to the electrodes
z = coordinate normal to x and y axis
z_1 = valency of cupric ion
α = thermal diffusivity
β = volumetric coefficient of expansion
δ = standard deviation
ν = kinematic viscosity
ρ = density
τ = dimensionless time
ϕ = inclination angle of the enclosure

Subscripts
a = anode
b = bulk or core
c = cathode
h = hot plate
s = solutal
t = thermal

Superscript
$^-$ = dimensionless quantity

I. Introduction

NATURAL convection in an enclosure has been a research subject creating much interest due to its diversive applications, e.g., the thermal insulations for building and solar collectors, the cooling systems for nuclear reactors, the convective processes in lakes, and the growth of crystals in semiconductor industry. The first systematic study with both theoretical and experimental analysis of natural convection flow in an enclosure at different inclinations was made by Hart.[1] His study was in a large aspect ratio and differentially heated rectangular box. Hart describes the base flow in terms of a parallel flow model with certain adjustable parameters. This has enabled him to carry out the stability analysis of the flow. Later on, studies on the stability of the flow for an inclined layer has attracted much research attention, and these studies can be grouped into three categories: 1) the effect of the Rayleigh number on the stability of different flow regimes and structure, especially the longitudinal rolls[2,3]; 2) the effect of the aspect ratio on the critical angle for transition of flow from longitudinal rolls to unicellular motion[4–6]; and 3) the Prandtl number effect on the stability of convection flow.[1,7] However, studies on the last category have not been well-documented. It is noted that the transition angle ϕ^* for flow from the longitudinal rolls to a transverse mode is generally characterized by a minimum in the Nusselt number on a $Nu - \phi$ plot.

Studies of heat transfer across an inclined enclosure at both low and moderate Rayleigh numbers have been reported and comprehensive reviews on this subject have been available.[8,9] Ayyaswamy and Catton[10] studied the heat transfer in the boundary-layer regime in the high aspect ratio enclosures and showed that when the Rayleigh number is sufficiently high, the heat transfer at different inclination can be obtained by

Received Aug. 30, 1993; revision received Nov. 17, 1994; accepted for publication Nov. 18, 1994.

*Professor, Institute of Aeronautics and Astronautics. Member AIAA.
†Graduate Student, Institute of Aeronautics and Astronautics.

using a simple rescaling of the results at $\phi = 90$ deg, as follows:

$$Nu(\phi) = Nu(\phi = 90 \text{ deg})\sin^{1/4}\phi \quad (1)$$

which is valid for 80 deg $\leq \phi \leq$ 180 deg. For an inclination angle at 0 deg $\leq \phi \leq \phi^*$, the $g \times \cos\phi$ scaling has been incorporated into the buoyancy force and more generalized correlations covering the entire Rayleigh number spectrum were obtained.

Natural convection heat transfer at high Rayleigh and Prandtl (Schmidt) numbers is not well-documented. Goldstein et al.[6,11] appear to be the first to use the same electrochemical system as the current one to study the effect of an inclination angle on the Sherwood number in a high aspect ratio (AR > 1) enclosure at both high Rayleigh and Schmidt number conditions. They found that the effect of AR increases dramatically when increasing the inclination angle. For an inclined enclosure, the $g \times \cos\phi$ scaling used for the heat transfer correlations works well for 0 deg $\leq \phi \leq$ 75 deg. At a given value of *Ra* and layer width, the Sherwood number decreases with increasing ϕ, and decreases sharply for ϕ close to and less than 90 deg. However, the flow structure was not visualized.

Visual observation of flow patterns and measurements of heat transfer in the inclined fluid layer have been made in a low aspect ratio (AR < 1) enclosure at high Grashof number conditions.[12] The experimental results indicated the occurrence of two corner cells on the sides for heating from below and unitary circulation cell in the core for heating from above. The Nusselt numbers, for heating from below, reduce with increasing the inclination angle. For heating from above, the Nusselt number results tend to collapse into a single curve in the range of *Gr* covered.

Most of the recent work mentioned in the preceding text has considered the thermal-induced convection in the inclined enclosures with AR > 1. Little attention has been paid to the solutal-induced convection flow and mass transfer in low aspect ratio (AR $\leq$ 1) inclined enclosures, especially at high *Sc* and *Ra* number conditions. Information for solutal convection in this configuration is lacking. In the present work a joint experimental and numerical study is performed to obtain the solutal convection flow structure and the mass transfer process in the low aspect ratio enclosures inclined at different angles. A comparison of flow structure between the data and the prediction will be made at $t = 30$ min when the mass transfer has reached steady state. The effect of both the inclination and the aspect ratio on the flow structure and mass transfer will be studied. The concentration fluctuations will be measured with a nonintrusive optical method. The Sherwood number across the enclosure at different inclinations will be measured, and the results will be correlated in terms of relevant nondimensional parameters.

II. Experimental Apparatus and Procedure

A. Experimental Apparatus

The rectangular test cell is made of 20-mm-thick Plexiglas® and has inside dimensions of 80 mm in height, 80 mm in width, and 47 mm in depth. Both of the vertical side walls of the enclosure are made of 12-mm-thick copper plate and serve as the electrodes. For the purpose of flow visualization, a smaller set of test cells is made that has inside dimensions of 20 mm in height, 20 mm in width, and 47 mm in depth.

A 25-mW He–Ne laser is employed as a light source for the measurement of concentration (fluctuations) in the solution. The light beam passing through the solution is partially absorbed. The change of light intensity, which according to Lambert–Beer's law is proportional to the magnitude of the local concentration of the solution, is measured with a power meter. To avoid the noise generation, however, a reference beam that is split from the original laser light is made. The reference beam is directed to pass through a similar test cell with no convection occurring inside. A differential amplifier is used to measure signal differences between the reference and the objective beam, which is a result of concentration oscillation in the test cell. By using the current apparatus, however, the noise that is generated can be completely eliminated.

The shadowgraph method is used primarily to visualize the interface shape and its location, and the solutal plume activity. The light beam from the 25-mW He–Ne laser is expanded with a spatial filter and is then collimated with a large diameter of plane convex lens. The collimated light passing through the region having a large variation of refractive index is deflected, and causes a shadow on the screen. The solutal plume and layer interface in the flow that have a relatively large variation of refractive index can be clearly observed. As an alternative, the polystyrene powder with diameter of 6 μm is used as a tracer to delineate and visualize the fluid motion. A Nikon FM2 camera with a 55-mm microlens is used for photographing.

B. Experimental Procedure

Since the electrode surfaces can become roughened due to a long period of deposition of cupric ion, they can be readily detached from the test cell for polish and cleaning. After the surface is cleaned, the prepared solution is carefully poured into the enclosure. Precautions are made to prevent an air bubble from being trapped inside. The entire test cell is placed on a platform that can be rotated and adjusted to ensure the test cell at the desired angle.

Before the experiment, the copper sulphate solution having a concentration from 0.02 to 0.1*M* is prepared. The amount of the distilled water is measured with a graduated cylinder. The copper sulfate powder is carefully weighed on a precision electronic balance, which has an accuracy of ± 0.001 g, and is then mixed with a given amount of distilled water to reach the desired concentration. Finally, the H_2SO_4 solution is added into the mixed solution as a supporting electrolyte. The concentration of H_2SO_4 is 1.5*M*. The thermal, chemical, and transport properties of the solution are well-documented.[13]

The electrolysis in the solution is initiated by switching on the dc power supply. A digital multimeter and a recorder were connected in parallel to the electronic circuit to measure the temporal variation of the potential and the current. To maintain the current density on the limiting current condition, the value of limiting current has to be measured before the experiment. The limiting current condition is determined by the potentiostatic-current method. The cell voltage is set with manual control in a stepwise manner, and the corresponding current is obtained and recorded. The procedure is repeated until the potential-current plateau is attained. More details on the limiting current measurement can be found in Ref. 13

To measure the mass transfer coefficient, the experiment is performed under the limiting current condition. This allows one to find the concentrations on both the cathode and the anode surfaces; the concentration on the cathode surface is zero, while that on the anode is twice the concentration of the bulk fluid. During the experiments, the limiting-current per unit area of the cathode can be measured and the mass transfer coefficient can be calculated by the following equation:

$$h_s = i_l/z_1 FC_b \quad (2)$$

where z_1 is the charge number of reacting ion.

III. Numerical Calculation

A. Mathematical Formulation

The current natural convection process is modeled with a two-dimensional cavity filled with an aqueous solution containing $CuSO_4 + H_2SO_4$. The coordinate system used is shown in Fig. 1. Both the top and the bottom walls are well-insulated.

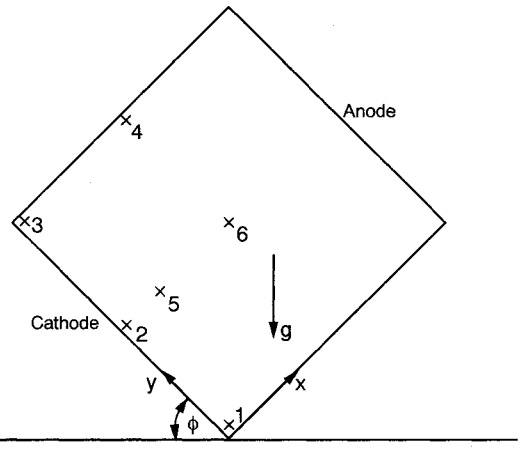

Fig. 1 Schematic diagram of the inclined enclosure and the locations for concentration fluctuation measurements.

For simplicity, all of the thermal transport properties, except for the density in the buoyancy force term, are assumed constant. In addition, the Boussinesq approximation is used. Initially, the working fluid is stagnant and has a uniform concentration. At time $t > 0$, natural convection is initiated by maintaining the concentration on one of the sidewalls at zero, and the opposite sidewall at $2C_b$. The development of the flow structure and transport process inside the cavity is described by a set of differential equations. Before the analysis, the governing equations are nondimensionalized with the following dimensionless parameters:

$$\bar{x} = x/H, \quad \bar{y} = y/H, \quad \tau = t/(H^2/D), \quad \bar{u} = u/(D/H)$$

$$\bar{v} = v/(D/H), \quad \bar{p} = p/(\rho D^2/H^2), \quad \bar{C} = (C - C_b)/C_b \tag{3}$$

$$\mathrm{AR} = H/L, \quad Sc = \nu/D, \quad Ra = \beta g C_b H^3/(\nu D)$$

Therefore, the nondimensionalized equations become as follows:

$$\frac{\partial \bar{u}}{\partial \bar{x}} + \frac{\partial \bar{v}}{\partial \bar{y}} = 0 \tag{4}$$

$$\frac{\partial \bar{u}}{\partial \tau} + \bar{u}\frac{\partial \bar{u}}{\partial \bar{x}} + \bar{v}\frac{\partial \bar{u}}{\partial \bar{y}} = -\frac{\partial \bar{p}}{\partial \bar{x}} + Sc\left(\frac{\partial^2 \bar{u}}{\partial \bar{x}^2} + \frac{\partial^2 \bar{u}}{\partial \bar{y}^2}\right) + RaScC\cos\phi \tag{5}$$

$$\frac{\partial \bar{v}}{\partial \tau} + \bar{u}\frac{\partial \bar{v}}{\partial \bar{x}} + \bar{v}\frac{\partial \bar{v}}{\partial \bar{y}} = -\frac{\partial \bar{p}}{\partial \bar{y}} + Sc\left(\frac{\partial^2 \bar{v}}{\partial \bar{x}^2} + \frac{\partial^2 \bar{v}}{\partial \bar{y}^2}\right) + RaScC\sin\phi \tag{6}$$

$$\frac{\partial \bar{C}}{\partial \tau} + \bar{u}\frac{\partial \bar{C}}{\partial \bar{x}} + \bar{v}\frac{\partial \bar{C}}{\partial \bar{y}} = \left(\frac{\partial^2 \bar{C}}{\partial \bar{x}^2} + \frac{\partial^2 \bar{C}}{\partial \bar{y}^2}\right) \tag{7}$$

Both the initial and the boundary conditions are the same as the experimental conditions. Before the experiments, the fluid inside the cell is stagnant and $\bar{C} = 0$. As the electrolysis is initiated, the concentration $\bar{C}$ on the cathode becomes 1, and on the anode it becomes -1.

B. Numerical Procedure

The governing equations are discretized using the control volume approach of Patankar.[14] In addition, the power law formulation is employed to determine the combined advective and diffusive fluxes across the boundaries of each control volume. The unsteady term is treated with backward difference. The buoyancy forces in the x-, y-momentum equations are treated as source terms. The conventional stagger grid system used originally in the SIMPLE scheme is adopted. The discretized equations are solved iteratively with the line-by-line procedure of tridiagonal matrix algorithm. To account for the drastic variations of the flow and concentration distribution during the initial transient period, a nonuniform time step is used. Depending on the Rayleigh number the $\Delta\tau$ in the beginning is set in a range from 1.74×10^{-7} to 1.74×10^{-6}, which corresponds to a real time from 0.031 to 0.31 s during the experiments.

Since the solutal boundary layer is confined in an extremely thin region along the wall, it is necessary to use a mesh that has very concentrated grids in the boundary layer and coarse grid in the core. The mesh used here is such that the first grid near the vertical wall has one-thousandth of the cavity width and the following grid expands at a rate of 10% until the solutal boundary-layer edge is reached. From the theoretical analysis,[15] the solutal boundary-layer thickness is given by $\delta_s \sim H/Ra^{1/4}$. The minimum value of δ_s for the current experimental conditions is 0.01 cm, which has a dimensionless thickness of 0.0041. Therefore, one could have a total of six grid points in the solutal boundary layer, the first grid has a mesh width of 0.0005 of the cavity width. This results in a grid system of 100×100 points in the entire enclosure.

Before numerical calculation, the modified numerical code was verified by comparing with a benchmark solution from De Vahl Davis[16] and a solution for natural convection of air in an enclosure.[15] The Nusselt number predicted using the current scheme agrees well with others at both low and high Rayleigh numbers.[15]

IV. Results and Discussion

A. Flow Visualization

The shadowgraph method allows one to observe and photograph the flow structure in an enclosure at different inclinations, as shown in Fig. 2, approximately 30 min after electrolysis has been initiated and the mass transfer process has reached steady state. For an inclination of 30 deg, a very strong solutal plume is initiated along both the top and the bottom layer. The plume that occurred has a semispherical-shaped end like a mushroom. The generation of solutal plume is due to the formation of a thin and lighter (heavier) layer of fluid near the cathode (anode) than the bulk, as a result of mass diffusion. When this layer becomes thicker and unstable at later times, it can protrude into the layer above (below), like the so-called thermals found in the thermal experiments.[17] For heating from below, the thermal plume found oscillates left and right. For Ra exceeding 10^6, this thermal plume does not rise up immediately once it is produced, but persists horizontally along the bottom plate for a certain distance. Similar phenomenon is also found in the current mass transfer experiment, except that the solutal plume is much thinner, like a finger. This is due to the relatively small rate of mass diffusion in comparison with the thermal diffusion. The persistent movement of solutal plume along the electrode surface and the protrusion of plume can increase the circulation motion of the core and enhance the mass transfer from the anode to the cathode.

Since the Schmidt number of the fluid is very high, the momentum boundary layer is much thicker than the solutal one. Therefore, a strong intrusion flow moving along the insulated plate can be produced by the viscous layer. The intrusion flow from the cathode (anode) is heavier (lighter) than the solutal boundary-layer flow. In addition, the bulk fluid is solutally stratified. As the intrusion flow moves along the insulated plate, it may reach an upper (lower) region where the surrounding fluid is lighter (heavier). At this stage, the intrusion flow is forced to turn downward (upward) and forms multistream of plumes. These plumes are slightly different from the ones generated along the electrode surface. They have no semispherical shape in the end and do not have a mushroom-like shape. The multistream of plumes was not

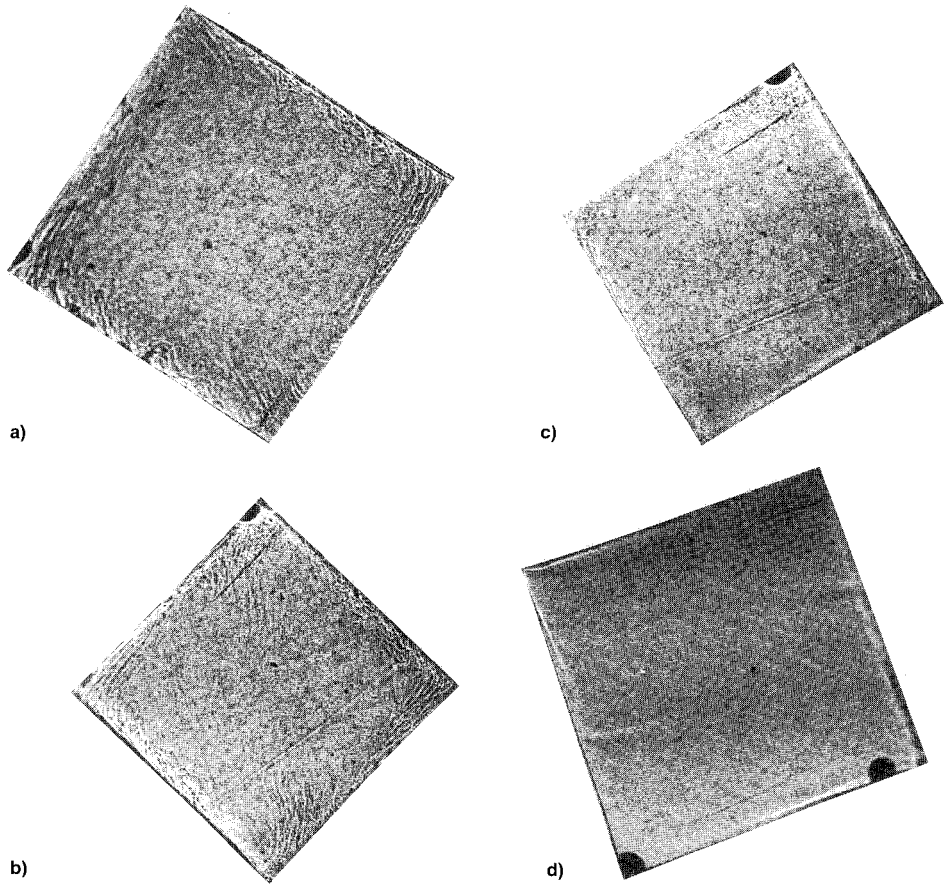

Fig. 2 Flow pattern by shadowgraph for AR = 1, $Ra = 3.53 \times 10^9$, $Sc = 2772$ and ϕ = a) 30, b) 45, c) 60, and d) 75 deg.

found in the thermal experiments. It is noted that both the solutal plumes and multistream formed are inherently three dimensional and highly unstable. The occurrence of these phenomenon is a problem of hydrodynamic instability. Therefore, it can be expected that even with a three-dimensional code, the occurrence of solutal plumes could not be properly predicted.

By increasing the angle of inclination, the solutal plume produced along the electrode tends to persist with the inclined wall (the cathode or the anode) for a longer distance, as shown in Fig. 2b for an inclined angle of 45 deg. In addition, the inclination of the plume produced near the insulated plate becomes higher. For an inclined angle of 60 deg, as shown in Fig. 2c, the solutal plume produced along the electrode is hardly observed except in the corner where it rises (descends) from the cathode (anode) and moves along the insulated wall. In addition, the multistream of plume produced along the insulated plate is completely absent. It appears that the angle of inclinaton at $\phi = 60$ deg is a critical one. For $\phi < 60$ deg, the flow structure appears like the one of heating from below in a horizontal enclosure. For $\phi > 60$ deg, it appears like the one of heating from the side in a vertical enclosure.

For the case when $\phi = 75$ deg, two-layer interfaces occur, which separate the core into three different layers, as shown in Fig. 2d. The occurrence of both the top and the bottom layer is attributed to the accumulation of solutal-layer flow. When the angle of inclination is large, the rate of solutal boundary-layer flow along the cathode (anode) entering the upper (bottom) region of the enclosure is greater than the mass flow along the anode (cathode) leaving that region. Since the rate of concentration diffusion is so small that mixing of the accumulated solutal layer flow with the bulk hardly occurs. This leads to the results that the accumulated flow separates sharply with the bulk and causes a density front in-between. The intrusion and accumulation of the solutal layer causes the growth of both the top and bottom layer. The sharp density front and the growth of the layer were not found in the thermal experiments. For a sufficiently long time, both the top and the bottom layer combine together and disappear, and the entire core becomes stratified.

Since the entire flow structure from the shadowgraph results is still not very clear, particle tracers are used to visualize the detailed structure of flow. The experimental results will then be compared, as shown in Figs. 3a–3c, for $t = 30$ min, with the prediction based on the SIMPLE algorithm. However, the plumes produced in the experiments could hardly be observed with this technique since they are very thin and occur in a random fashion. The streaks shown in Fig. 3 have 25-s exposures. Since the variations of flow structure with time at $t = 30$ min are very slow, the streakline photographed is nearly equal to the streamline. However, the solutal plumes were not found either in the photograph of the streakline or the prediction of the streamline. This is due to the fact that in the experiments the plumes that were produced could hardly be observed with particle tracers since they are very thin and occur in a random fashion. On the other hand, the numerical calculation could not predict the problem of flow instability as mentioned previously. Despite this discrepancy, the agreement between the data and the prediction for the entire bulk flow is very good.

For $\phi = 30$ deg, the entire enclosure, except in the top and the bottom corner, is filled with a clockwise cell with two symmetric, small clockwise cells enclosed inside. When the angle of inclination increases, both the large cell outside and the two small cells inside the enclosure decrease in size, as shown in Fig. 3b for $\phi = 60$ deg. This is due to the fact that the circulation motion of the core is driven mostly by the solutal layer on the sides. As the angle of inclination ϕ is small, due to the vertical buoyancy, the solutal layer tends to move or protrude into the core and produce a more rapid

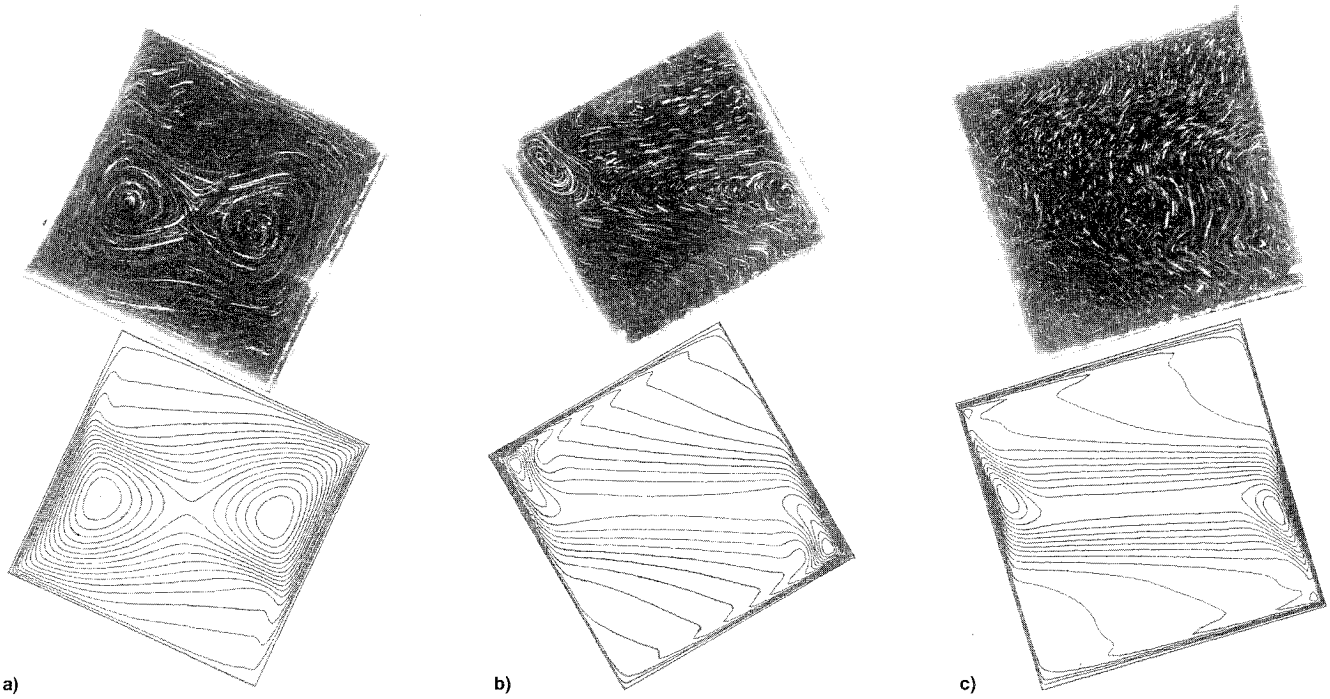

Fig. 3 Comparison of flow structure between experimental observation and prediction for AR = 1, $Ra = 3.53 \times 10^9$, $Sc = 2772$ and ϕ = a) 30, b) 60, and c) 75 deg.

and large circulation of the core. As ϕ is large, however, the solutal layer tends to be confined in a very thin region close to the side wall and could not effectively drive the core and produce a large cell. This leads to a result that the circulation motion of the core becomes weaker, and the mass transfer rate across the enclosure becomes smaller. Outside the cell as the vertical boundary layer detrains, flow reversal occurs. The reversal of boundary-layer flow can also be observed in the photograph, which becomes more evident as ϕ becomes large and circulation cells in the core shrink.

For $\phi = 75$ deg, the large circulation cell in the core becomes weaker. The two small cells inside do not shrink further, but move toward the central region like a secondary cell. The flow structure at the current stage is very much like the case for $\phi = 90$ deg. The lighter (heavier) solutal-layer flow accumulates layer-by-layer in the top (bottom) corner and forms a layer interface at the edge connecting with the bulk, as shown in the previous shadowgraph. The flow accumulated in both the top and the bottom region is nearly stagnant and stratified, which can also be concluded in the prediction of the streamline plot as shown in Fig. 3c and the isoconcentration line.[15] With careful examination, the interface location inferred in the prediction is actually very close to that indicated in the photograph of Fig. 2d. It appears that the numerical algorithm used can accurately predict the buoyancy-induced convection of a high Schmidt number of fluid. On the other hand, it can also be concluded that the electrochemical system used and the boundary condition created at the electrode surface are very close to an ideal situation that was assumed in the numerical calculation. The stratified region in both the top and the bottom portion of the enclosure can significantly reduce the mass transfer. This can also be confirmed in the mass transfer measurement in the following sections.

B. Concentration Oscillation Measurements

The concentration measurements are performed 30 min after the electrolysis has been initiated (and the mass transfer process has reached steady state). A total of six measurement locations has been selected (Fig. 1): 1) 0.05, 0.05; 2) 0.05, 0.5; 3) 0.05, 0.95; 4) 0.5, 0.95; 5) 0.15, 0.5; and 6) 0.5, 0.5, where concentration oscillation may occur. Points 1–3 are located very close to the edge of the solutal boundary layer. For the case when $\phi = 30$ deg, a very large amplitude and high frequency of oscillation is found at points 2 and 3, as shown in Figs. 4b and 4c, where plume activity is very intense. It appears that the concentration oscillation measured is mostly due to the rise of the lighter plume or the falling of the heavier plume. At point 1 (Fig. 4a), which is near the leading edge of the boundary layer where plume activity is hardly observed, no oscillation in concentration is found. At points 4 and 5, which are far from the edge of the solutal boundary layer, the number of plumes generated passing through these locations becomes less. In addition, due to mass diffusion, the plume arriving at this location has the concentration close to the bulk. This leads to a result that both the amplitude and the frequency of the concentration oscillation reduce significantly, as shown in Figs. 4d and 4e. At point 6, which is located at the center of the core where no plume activity is found as shown in the previous figure, the concentration oscillation is not observed as shown in Fig. 4f.

By increasing the angle of inclination, the plume activity decreases. For $\phi = 60$ deg, the most intense activity of plume occurs at the corner close to point 3. This causes a relatively large amplitude and high frequency of concentration oscillation.[15] At other points where plume activity is much less, the concentration oscillations become weaker.[15] No plume activity and concentration oscillation is found at points 5 and 6. For $\phi > 60$ deg, both the plume activity and the concentration oscillation are not found. In the numerical calculation, however, the concentration fluctuations were not found, due to its inability to calculate the occurrence of the solutal plumes.

C. Mass Transfer

For different aspect ratio of enclosures, the variations of the Sherwood numbers with enclosure inclination are measured and plotted in Fig. 5. Both the minimum and the maximum in Sherwood number that occur in the thermal experiments[4,18,19] are not found. The minimum in Nusselt number occurs when a transition of flow structure from a series of roll-cells to a single roll-cell occurs. For a very high aspect ratio of enclosure, Goldstein et al.[6] measured the Sherwood

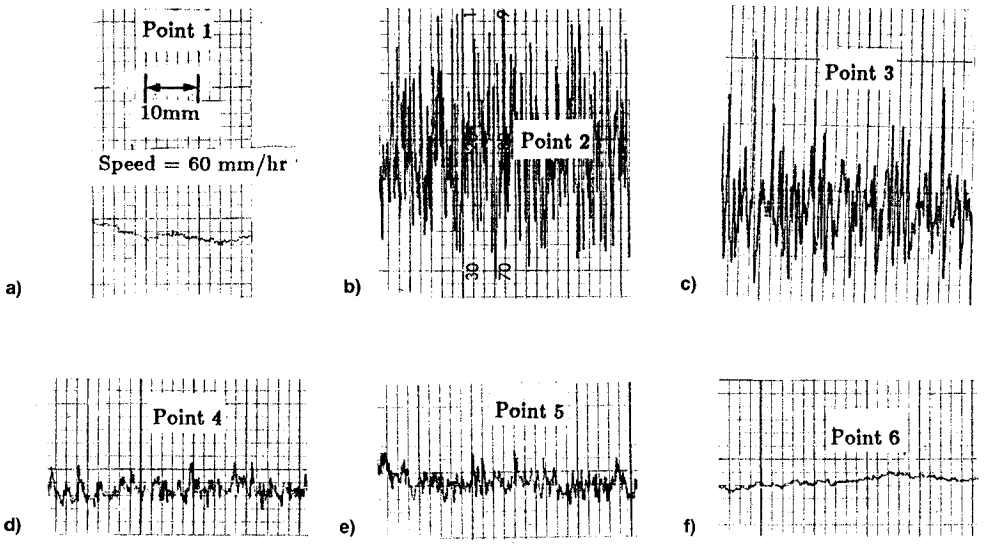

Fig.4 Concentration fluctuations for ϕ = 30 deg, AR = 1, Ra = 3.53 × 10^9, and Sc = 2772 at point a) 1 (0.05, 0.05); b) 2 (0.05, 0.5); c) 3 (0.05, 0.95); d) 4 (0.5, 0.95); e) 5 (0.15, 0.5); and f) 6 (0.5, 0.5).

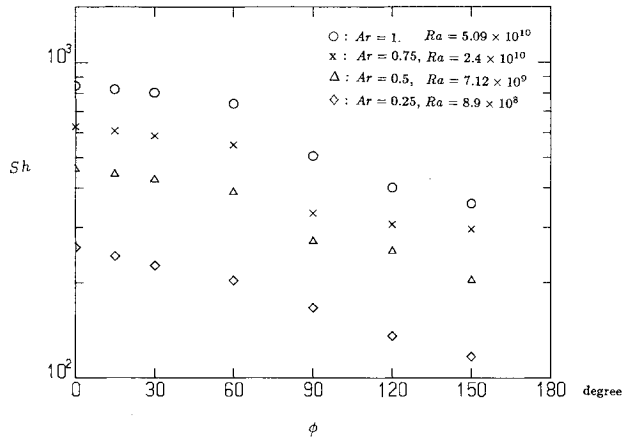

Fig. 5 Variations of Sherwood number with inclination of the enclosure at different aspect ratios.

number in the same electrochemical system as the current one, and found that a sharp decrease in the Sherwood number occurs at approximately ϕ = 85 deg. They suspect a change of flow structure and occurrence of minimum in Sherwood number at that angle. The critical angle does not change when the aspect ratio reduces and is close to 1.8. However, Ozoe et al.[4] found that as the aspect ratio of enclosure decreases, the minimum in Nusselt number occurs at a smaller angle of inclination. For aspect ratio of unity, the minimum in Nusselt number occurs at approximately ϕ = 10 deg. For current mass transfer system in an enclosure with AR ≤ 1, the minimum in Sherwood number is expected to occur at ϕ < 10 deg. Due to lack of data, however, this could not be concluded from the Sherwood number distribution of Fig. 5.

In the thermal experiments,[4] however, the maximum in Nusselt number at a critical angle also occurs. For aspect ratio of unity, the maximum in Nusselt number occurs approximately at ϕ = 60 deg. However, in the electrochemical system of a high Schmidt number of fluid with AR > 1.8,[6,11] the maximum Sherwood number does not appear. This is also true in the current system for AR ≤ 1. The Sherwood number decreases monotonically from ϕ = 0 to 150 deg. The largest value of Sherwood number occurs approximately at ϕ = 0 deg, where intense activity of solutal plume occurs. In addition, the lighter (heavier) boundary-layer flow tends to move upward (downward) along the inclined bottom (top) wall, which results in a thinner solutal layer and higher mass transfer rate. As the inclination of the enclosure ϕ is greater than 60 deg, the Sherwood number for AR close to unity decreases rapidly, as shown in Fig. 5. The solutal plume at this stage has diminished completely. In addition, the lighter (heavier) solutal boundary-layer flow gradually accumulates and stratifies along the top (bottom) region. The two stratified layers in both the top and the bottom region grow gradually, which can significantly suppress both the momentum and the solutal layer flow and reduce the mass transfer rate. In a low aspect ratio enclosure (AR = 0.25), where the core flow has been very slow, the stratification of both the top and the bottom layer could not further suppress in a significant amount the solutal boundary-layer flow. Therefore, no sharp decrease in the Sherwood number occurs at ϕ > 60 deg.

For the case with ϕ > 90 deg, the increase of inclination angle causes the buoyancy force, which drives the solutal boundary-layer flow along the inclined wall, to decrease. This results in a slower motion of boundary-layer flow and a rapid decrease in the mass transfer.

All the Sherwood numbers measured at different experimental conditions are listed in Table 2 of Ref. 15. During the experiments, the dimensionless parameter for the Ra number varies from 10^8 to 10^{11}, the aspect ratio from 0.25 to 1, the Schmidt number from 2.5 × 10^3 to 3.0 × 10^3, and the inclination ϕ from 30 to 150 deg. Correlations of Sherwood number with relevant nondimensional parameters at different angles of inclination are made, which are listed in Table 1. Since the aspect ratio may have a significant effect on the mass transfer rate, the first attempt was made to correlate the Sh number with both the Rayleigh number and the aspect ratio. The results are shown at the second column in Table 1. At ϕ = 30 deg, the Sh number varies linearly with $Ra^{0.316}$. The power of 0.316 suggests that the flow may not completely be laminar due to the plume activity. As the inclination ϕ increases, which is accompanied with the decrease in plume activity, the power of Ra in the correlation decreases. As ϕ > 60 deg, where the plume activity has completely diminished and stratification in both the upper and the lower region occurs, the power of Ra becomes very close to one-quarter, which is the characteristic of a laminar natural convection. The small value for the power of AR in the correlations suggests that the effect of the aspect ratio on the mass transfer rate is very small and can be neglected. In the third column of Table 1, the Sh number is correlated only with the Rayleigh number and the correlation results are very satisfactory. Comparison of the correlations with the data is shown in Fig. 6.

Table 1 Least-square-fit of the data at different inclination angles

Angle of inclination	Two-parameter correlation	One-parameter correlation
30	$Sh = 0.349Ra^{0.316}(\mathrm{AR})^{-0.05}$ $\delta = 0.123$	$Sh = 0.379Ra^{0.3095}$ $\delta = 0.0189$
60	$Sh = 0.349Ra^{0.309}(\mathrm{AR})^{-0.019}$ $\delta = 0.127$	$Sh = 0.368Ra^{0.3034}$ $\delta = 0.0209$
90	$Sh = 0.443Ra^{0.252}(\mathrm{AR})^{0.025}$ $\delta = 0.097$	$Sh = 0.414Ra^{0.255}$ $\delta = 0.0173$
120	$Sh = 0.42Ra^{0.248}(\mathrm{AR})^{-0.01}$ $\delta = 0.0088$	$Sh = 0.433Ra^{0.247}$ $\delta = 0.014$
150	$Sh = 0.32Ra^{0.254}(\mathrm{AR})^{0.005}$ $\delta = 0.109$	$Sh = 0.324Ra^{0.254}$ $\delta = 0.025$

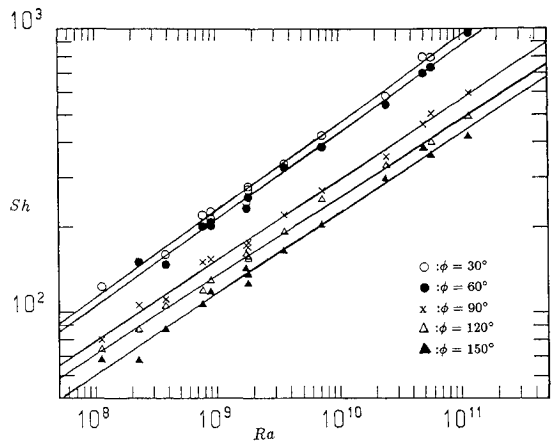

Fig. 6 Correlation of *Sh* with *Ra* for inclination angles from 30 to 150 deg.

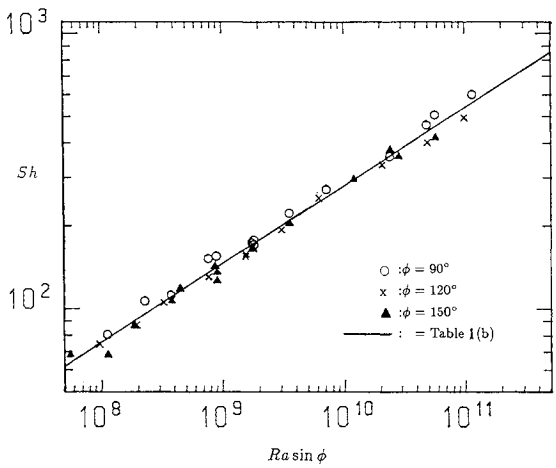

Fig. 7 Correlation of *Sh* with *Ra* sin ϕ for 90 deg $\leq \phi \leq$ 150 deg.

All the data and the correlations indicate a significant decrease in the *Sh* number as the inclination angle increases from 60 to 90 deg, where plume activity diminishes completely and stratification in both the upper and the lower region occurs.

A single correlation for all the heat transfer data at ϕ less than 90 deg has been obtained in the thermal experiments[20] if the Nusselt number is correlated with *Ra* cos ϕ. In addition, for a high aspect ratio enclosure, a single correlation of *Sh* number with *Ra* cos ϕ is also obtained for 0 deg $< \phi <$ 60 deg (Ref. 6). This suggests that in the current low aspect ratio system the *Sh* number at both ϕ = 30 deg and ϕ = 60 deg can be correlated with *Ra* cos ϕ, and the result is obtained as follows:

$$Sh = 0.437(Ra \cos \phi)^{0.307} \quad (8)$$

The least-square-fit of data has a standard deviation of 0.0289. The correlation result is good. For the case with $\phi > 90$ deg, an attempt was made to correlate *Sh* number with *Ra* sin ϕ. This has been achieved in thermal experiments for *Pr* = 0.7 and AR in the range from 5 to 83 (Ref. 20). The correlation for the current data is very successful, and the result is written as follows:

$$Sh = 0.302(Ra)^{0.254} \sin \phi \quad (9)$$

The least-square-fit of the data has a standard deviation of 0.0384. Comparison between the correlation and the data is shown in Fig. 7.

V. Conclusions

A joint experimental and numerical work is performed to study the solutal convection flow and mass transfer in an enclosure inclined at different angles. The good agreement of flow structure between the experimental observation and the prediction indicates that the current electrochemical system can be used to study experimentally the buoyancy-induced convection in a enclosure. Both the data and the prediction indicate that the inclination of the enclosure can significantly change the flow structure and affect the mass transfer process. For large angles of inclination, the solutal boundary-layer flow can accumulate and stratify along both the upper and the lower region of the enclosure and reduce the mass transfer. At small angles of inclination, however, the solutal boundary-layer flow becomes unstable and generates solutal plume that can protrude into the core and enhance the mass transfer. In addition, the random protrusion of the plume causes strong oscillations of concentration. Since the solutal plume could not be simulated numerically, the computation may later lead to an erroneous result.[15]

The Sherwood numbers at different inclination and aspect ratios of the enclosure are measured, which decrease monotonically when increasing the inclination angle. By using proper nondimensional parameters and scaling, a single correlation of the Sherwood number, covering the entire range of *Ra* and AR studied experimentally, can be obtained for an inclination angle less or greater than 90 deg.

References

[1]Hart, J. E., "Stability of the Flow in a Differentially Heated Inclined Box," *Journal of Fluid Mechanics*, Vol. 47, June 1971, pp. 547–576.

[2]Unny, T. E., "Thermal Instability in Differentially Heated Inclined Fluid Layers," *Journal of Applied Mechanics*, Vol. 39, No. 1, 1972, pp. 41–46.

[3]Clever, R. M., and Busse, F. H., "Instabilities of Longitudinal Convection Rolls in an Inclined Layer," *Journal of Fluid Mechanics*, Vol. 81, June 1977, pp. 107–127.

[4]Ozoe, H., Sayama, H., and Churchill, S. W., "Natural Convection in an Inclined Rectangular Channel at Various Aspect Ratio and Angles-Experimental Measurements," *International Journal of Heat and Mass Transfer*, Vol. 18, No. 12, 1975, pp. 1425–1431.

[5]Arnold, J. N., Catton, I., and Edward, D. K., "Experimental Investigation of Natural Convection in Inclined Rectangular Regions of Differing Aspect Ratios," *Journal of Heat Transfer*, Vol. 98, No. 1, 1976, pp. 67–71.

[6]Goldstein, R. J., Chiang, N. D., and Sayer, E., "Natural Convection Mass Transfer in an Inclined Enclosure at High Rayleigh Number," *2nd International Symposium on Transport Phenomena in Flows* (Tokyo), 1987, pp. 229–255.

[7]Korpela, S. A., "A Study of the Effect of Prandtl Number on the Stability of the Conduction Regime of Natural Convection in an Inclined Slot," *International Journal of Heat and Mass Transfer*, Vol. 17, No. 2, 1974, pp. 215–222.

[8]Catton, I., "Natural Convection in Enclosure," *Proceedings of the Sixth International Heat Transfer Conference*, Vol. 6, 1978, pp. 11–13.

[9]Ostrach, S., "Natural Convection in Enclosure," *Advances in Heat Transfer*, edited by J. P. Hartnett and T. F. Irvine, Vol. 8, 1972, pp. 161–227.

[10]Ayyaswamy, P., and Catton, I., "The Boundary-Layer Regime for Natural Convection in a Differentially Heated, Tilted Rectangular Cavity," *Journal of Heat Transfer*, Vol. 95, No. 4, 1973, pp. 543–545.

[11]Goldstein, R. J., Chiang, H. D., and See, D. L., "High Rayleigh-Number Convection in a Horizontal Enclosure," *Journal of Fluid Mechanics*, Vol. 213, April 1990, pp. 111–126.

[12]Wang, L. W., Chai, A., and Rashidnia, N., "Ground-Based Experiments on Thermal and Thermosolutal Convection in Inclined Low-Aspect-Ratio Enclosures," AIAA Paper 90-0413, Jan. 1990.

[13]Wilke, C. R., Eisenberg, M., and Tobias, C. W., "Correlation of Limiting Current Under Free Convection Condition," *Journal of Electrochemical Society*, Vol. 100, No. 11, 1953, pp. 513–523.

[14]Patankar, S. V., *Numerical Heat Transfer and Fluid Flow*, Hemisphere, New York, 1980.

[15]Jeng, D. Z., "Experimental and Numerical Study of Steady State and Transient Natural Convection in Inclined Enclosures," Ph.D. Dissertation, National Cheng Kung University, Taiwan, ROC, 1992.

[16]De Vahl Davis, G., "Natural Convection of Air in a Square Cavity: A Bench Mark Solution," *International Journal of Numerical Methods in Fluids*, Vol. 3, No. 3, 1983, pp. 249–264.

[17]Goldstein, R. J., and Chu, T. Y., "Thermal Convection in a Horizontal Layer of Air," *Progress in Heat and Mass Transfer*, Vol. 27, 1984, pp. 55–75.

[18]Hollands, K. G. T., Raithby, G. D., and Konicek, L., "Correlation Equations for Free Convection Heat Transfer in Horizontal Layer of Air and Water," *Journal of Heat Transfer*, Vol. 97, No. 7, 1976, pp. 884–887.

[19]Ruth, D. W., Hollands, K. G. T., and Raithby, G. D., "On Free Convection Experiments in Inclined Air Layer Heated from Below," *Journal of Fluid Mechanics*, Vol. 96, Feb. 1980, pp. 461–479.

[20]Inaba, H., "Experimental Study of Natural Convection in an Inclined Air Layer," *International Journal of Heat and Mass Transfer*, Vol. 27, No. 8, 1984, pp. 1127–1139.